

Draft processed June 25, 2019

# Excitation and Disruption of a Giant Molecular Cloud by the Supernova Remnant 3C 391

William T. Reach<sup>1</sup>

Infrared Processing and Analysis Center, California Institute of Technology, Pasadena, CA 91125

Jeonghee Rho<sup>2</sup>Service d'Astrophysique, CEA, DSM, DAPNIA, Centre d'Etudes de Saclay, F-91191  
Gif-sur-Yvette cedex, France

## ABSTRACT

Using the IRAM 30-m telescope, we observed the supernova remnant 3C 391 (G31.9+0.0) and its surroundings in the  $^{12}\text{CO}(2 \rightarrow 1)$ ,  $\text{HCO}^+(1 \rightarrow 0)$ ,  $\text{CS}(2 \rightarrow 1)$ ,  $\text{CS}(3 \rightarrow 2)$ , and  $\text{CS}(5 \rightarrow 4)$  lines. The ambient molecular gas at the distance of the remnant comprises a giant molecular cloud whose edge is closely parallel to a ridge of bright non-thermal radio continuum, which evidently delineates the blast-wave into the cloud. We found that in a small (0.6 pc) portion of the radio shell, the molecular line profiles consist of a narrow ( $2 \text{ km s}^{-1}$ ) component, plus a very wide ( $> 20 \text{ km s}^{-1}$ ) component. Both spectral components peak within  $20''$  of a previously-detected OH 1720 MHz maser. We name this source 3C 391:cs; it provides a new laboratory, similar to IC 443 but on a larger scale, to study shock interactions with dense molecular gas. The wide spectral component is relatively brighter in the higher-excitation lines. We interpret the wide spectral component as post-shock gas, either smoothly accelerated or partially dissociated and reformed behind the shock. The narrow component is either the pre-shock gas or cold gas reformed behind a fully dissociative shock. Using the 3 observed CS lines, we measured the temperature, CS column density, and  $\text{H}_2$  volume density in a dense clump in the parent molecular cloud as well as the wide-line and narrow-line portions of the shocked clump. The physical conditions of the narrow-line gas are comparable to the highest-density clumps in the giant molecular cloud, while the wide-line gas is *both* warmer and denser. The mass of compressed gas in 3C 391:cs could be high enough that its gravity would be significant, and eventually it should form one or several stars.

*Subject headings:* supernova remnants, ISM: individual (3C 391), ISM: structure, radio lines: ISM

---

<sup>1</sup>formerly: Institut d'Astrophysique Spatiale, Bâtiment 121, Université Paris XI, 91405 Orsay cedex, France

<sup>2</sup>currently: Physics Department, University of California, Santa Barbara, CA

## 1. Introduction

Supernovae are thought to be the source of kinetic energy of the interstellar medium, keeping the gas in motion and returning material from dense molecular clouds into the more diffuse interstellar medium and the galactic halo. When a massive star ends its life in a supernova explosion, it often does so in the vicinity of the molecular cloud in which it was born, as is evidenced by the close correspondence of OB associations and giant H II regions in spiral arms (Elmegreen & Lada 1977). Despite the expected close association between Type II supernovae and molecular clouds, very few cases of supernova-molecular cloud (SN-MC) interaction are known or suspected. The blast wave from a supernova within or near the edge of a cloud will progress rapidly through the inter-clump medium and drive slower shocks into dense clumps. Multiple reflections of high-energy charged particles within the complicated magnetic field of an SN-MC interaction are a possible source of cosmic rays, which will permeate the entire region (Chevalier et al. 1977; Esposito et al. 1996). The thermal radiation from the remnant interior (mainly X-rays), cosmic rays and their secondary gamma rays, and direct impact of the blast wave onto clumps should visibly perturb the excitation, chemistry, and dynamics of the parent molecular cloud for at least the  $\sim 10^5$  year period during which the SN blast wave is most powerful.

So far, the only well-known case of an SN-MC interaction is IC 443, where molecular lines have been detected with  $\text{FWHM} \sim 20 \text{ km s}^{-1}$  (much wider than the lines from nearby, un-shocked gas), and from energy levels far above the ground state (White et al. 1987; van Dishoeck, Jansen, & Phillips 1993; Wang & Scoville 1992). Other remnants, including W 28, CTB 109, Kes 79, and W 51C have been suggested as SN-MC interactions based on their proximity to molecular clouds, wide molecular lines, or both (Wootten 1977; Wootten 1981; Tatematsu et al. 1990; Green & Dewdney 1992; Koo & Moon 1997a; Koo & Moon 1997b). In the case of W 28, W 44 and 3C 391, 1720 MHz OH emission has been detected from many small spots, with brightness temperatures so high that they must be masers; these masers are thought to be collisionally excited and they strongly suggest the presence of SN-MC interactions (Frail, Goss, & Slysh 1994; Frail et al. 1996). 3C 391 is one of the brightest radio supernova remnants, and high-resolution radio images suggest a ‘break-out’ morphology due to an explosion near the edge of a molecular cloud (Reynolds & Moffett 1993). The X-ray emission from 3C 391 peaks in its interior and has a thermal spectrum (Rho & Petre 1996), characteristic of a newly-defined class of supernova remnants, called ‘mixed-morphology’ remnants, whose nature has been linked to interaction with a strongly inhomogeneous pre-shock interstellar medium (Rho & Petre 1998). A recent map of the  $^{12}\text{CO}(1 \rightarrow 0)$  emission in the vicinity of 3C 391 revealed a giant molecular cloud that is precisely parallel to the bright ridge of radio emission, confirming that its ‘break-out’ radio morphology is indeed due to the strong density contrast between the molecular cloud to the northwest and the relatively empty regions elsewhere (Wilner, Reynolds, & Moffett 1998). The work described in this paper is part of our recently-initiated campaign to search for and characterize SN-MC interactions in the mixed-morphology supernova remnants. Our first result was the detection of bright [O I] 63  $\mu\text{m}$  and dust emission from 3C 391, showing that the blast-wave into the molecular

gas is radiative, and the SN-MC interaction is a significant energy loss for the remnant, although it remains globally adiabatic (Reach & Rho 1996). In this paper, we present new observations of molecular emissions from 3C 391, designed to search for the effects of the SN-MC interaction on the molecular cloud, using millimeter-wave observations at high angular resolution and several transitions requiring a range of physical conditions for excitation.

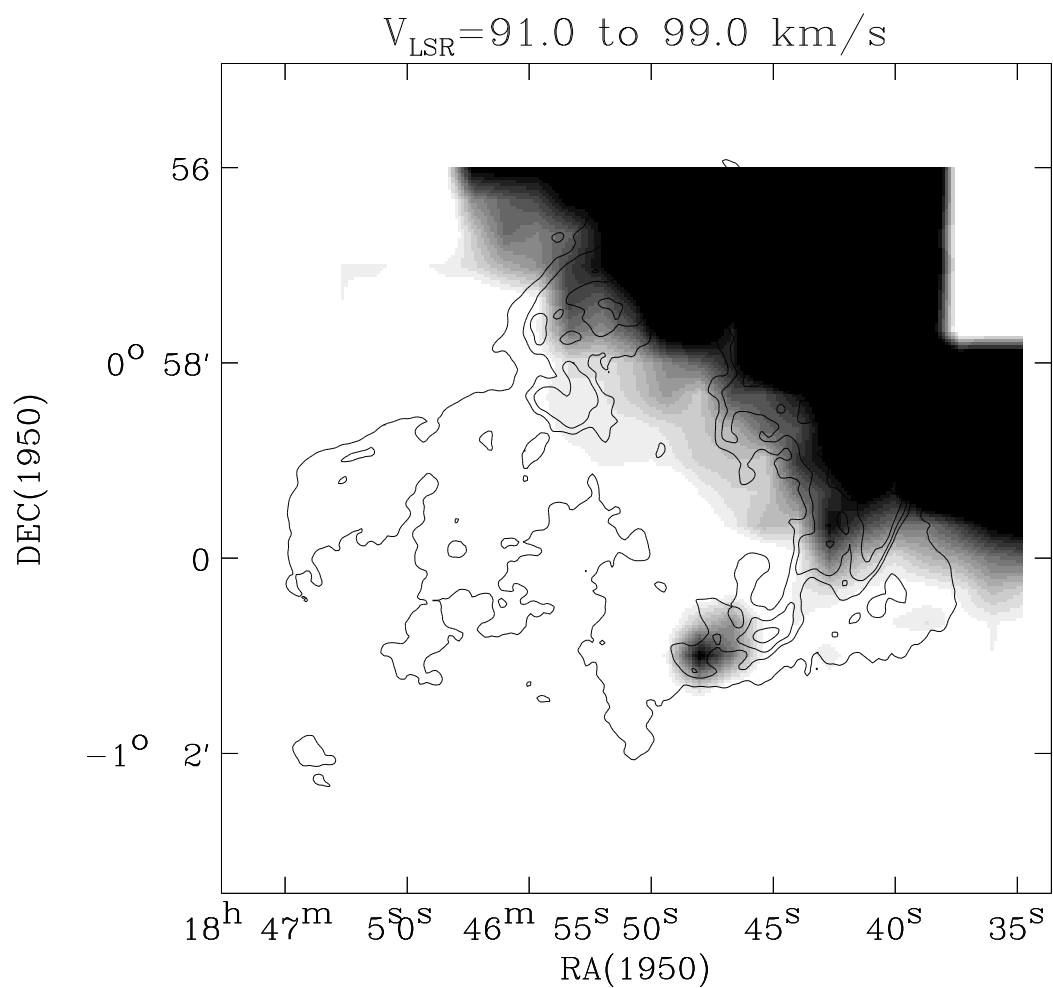
## 2. Observations and Results

The observations described here were made with the IRAM 30-m telescope during 22–27 November 1996, in very good weather. Three receivers were used to simultaneously observe three different spectral lines with the 1.3, 2, and 3 mm receivers. Our most-used receiver configuration contained the  $^{12}\text{CO}(2 \rightarrow 1)$ ,  $\text{CS}(3 \rightarrow 2)$ , and  $\text{CS}(2 \rightarrow 1)$  lines. Part of the time, we switched the 1.3 mm receiver to the  $\text{CS}(5 \rightarrow 4)$  line, and part of the time, we switched the 3mm receiver to the  $\text{HCO}^+(1 \rightarrow 0)$  line. The transitions, frequencies, telescope efficiencies, and beam-widths (from Wild 95) are shown in Table 1. Both the autocorrelator and filter-banks were used as back-ends, the former allowing good velocity resolution and the latter used to cover a wide range of velocities. Wide velocity coverage was particularly important so that we could search for very broad lines and differentiate frequency-dependent gain variations of the receiver from the true spectral shape of our source. Positions in the this paper will be expressed as offsets, relative to a central position (epoch 1950) of  $18^{\text{h}}46^{\text{m}}50^{\text{s}}$   $-1^{\circ}00'00''$ . Each spectrum is the brightness relative to a reference position, which was offset from the central position by  $+255'', -300''$  in r.a., dec, respectively. It was not possible to find a reference position close to the remnant that was devoid of CO line emission, but using the  $^{12}\text{CO}(1 \rightarrow 0)$  map (Wilner et al. 1998), we were able to find a position with very low total emission and no emission at all at the velocities appropriate for gas at the distance of 3C 391. There is a negative dip in the  $^{12}\text{CO}(2 \rightarrow 1)$  spectra at  $40 \text{ km s}^{-1}$  due to contamination from the reference position. All spectral lines at velocities lower than  $50 \text{ km s}^{-1}$  are not related to the remnant and can be ignored.

## 3. Distribution of Ambient Molecular Gas near 3C 391

We mapped the entire remnant and surroundings on a  $20''$  grid, and then we mapped the region where we found wide molecular lines on a  $10''$  grid. The relationship between the nonthermal radio emission of the supernova remnant and the overall distribution of molecular gas at the same distance is shown in Figure 1. The  $^{12}\text{CO}(2 \rightarrow 1)$  line was integrated over the velocity range  $91\text{--}99 \text{ km s}^{-1}$ , and the contours of radio continuum surface brightness (from Reynolds & Moffett 1993) are superposed. The CO emission is very bright to the northwest if the remnant, with the edge of the bright region running precisely along the radio shell of the supernova remnant. The  $^{12}\text{CO}(1 \rightarrow 0)$  emission, mapped over a larger area by Wilner et al. (1998), shows that the molecular cloud boundary continues outside the boundaries of our map. Looking on even

Fig. 1.— An overlay of the  $^{12}\text{CO}(2 \rightarrow 1)$  brightness (integrated over the velocity range 91–99  $\text{km s}^{-1}$ ) on the radio contours. The CO observations are sampled every  $20''$ . The region of bright CO emission to the northwest is most likely the parent cloud of the 3C 391 supernova progenitor.



larger scales, in the Massachusetts-Stony Brook CO survey (Clemens et al. 1986), the CO emission spans an irregular region about  $15'$  minutes across. Part of this region was identified as a giant molecular cloud with  $(l, b, v) = (32.00^\circ, 0.00^\circ, 98 \text{ km s})$ ,  $(\sigma_l, \sigma_b, \sigma_v) = (0.22, 0.09, 3.0)$ , and its virial mass was estimated to be  $4 \times 10^5 M_\odot$  (Solomon et al. 1987). Including other molecular emission that seems associated, the total mass of the complex is perhaps twice as high. The  $^{12}\text{CO}(2 \rightarrow 1)$  and  $\text{CS}(2 \rightarrow 1)$  maps, and the  $^{12}\text{CO}(1 \rightarrow 0)$  map of a larger region (Wilner et al. 1998), all show that the bright northeastern radio shell of 3C 391 is nearly tangent to the surface of this molecular cloud. The radio, X-ray, and mm-wave CO-line morphologies suggest that 3C 391 is the result of an explosion near the edge of a giant molecular cloud. We will call this cloud the ‘parent cloud’, because it is likely that the progenitor was a massive star that formed in or near the cloud, but this term is merely suggestive for the purposes of this paper.

Over nearly the entire region shown in Figure 1, the detected lines are all *narrow*, with  $\text{FWHM} < 3.5 \text{ km s}^{-1}$ . Two example spectra, toward the peak of the nonthermal radio shell a bright position in the parent molecular cloud, are shown in Figures 2 and 3, respectively. The  $^{12}\text{CO}(2 \rightarrow 1)$  line is detected almost everywhere, and the  $\text{CS}(2 \rightarrow 1)$  and  $\text{CS}(3 \rightarrow 2)$  lines are detected inside the boundary of the parent molecular cloud, which is to say, in the northwestern corner of the map (Fig. 3b). The parent cloud is not uniform—it contains several clumps, which are more pronounced in the CS maps. We identified a bright clump in the parent molecular cloud, at  $(-150'', 220'')$ , for comparison with the physical properties of the shocked gas. The ambient cloud has relatively weak  $\text{CS}(3 \rightarrow 2)$  emission and undetectable ( $< 0.1 \text{ K}$ )  $\text{CS}(5 \rightarrow 4)$  emission.

#### 4. Molecular Spectra of a Shocked Clump

The molecular emission lines change radically from those of the parent molecular cloud in one small region, near one of the two OH masers found in 3C 391 (Frail et al. 1996) at  $18^{\text{h}}46^{\text{m}}47.69^{\text{s}}$ ,  $-01^\circ 01' 00.6''$ . Every molecular transition we observed was significantly broadened within a small patch of sky, about  $1'$  in diameter. The spectra taken towards two positions, only  $45''$  apart, are shown in Figure 4. There are two components of the spectral lines, wide and narrow, which have very different relative brightnesses in different transitions. The wide component of the spectral lines in Figure 4 has a full width at half maximum (FWHM) of  $20 \text{ km s}^{-1}$ , while the narrow component has a FWHM of only  $1.7 \text{ km s}^{-1}$ . The  $\text{CS}(2 \rightarrow 1)$  line integral toward this clump is  $400 \text{ K km s}^{-1}$ , which is an order of magnitude larger than the typical line integral from the parent molecular cloud. The central velocity of the *narrow* component is the same as that of the OH 1720 MHz maser line (Frail et al. 1996), but the center of the wide component is somewhat offset (but by much less than the line width). Because the properties of the molecular emission in this region are so very different from those typical of the molecular gas in the region, and the position coincides with a shock-excited OH maser and the [O I]  $63 \mu\text{m}$  emission peak, we conclude that this is a region where the supernova blast-wave has had a significant impact on the molecular gas. We will therefore refer to this region as the ‘shocked clump,’ or 3C 391:cs, and we will attempt to

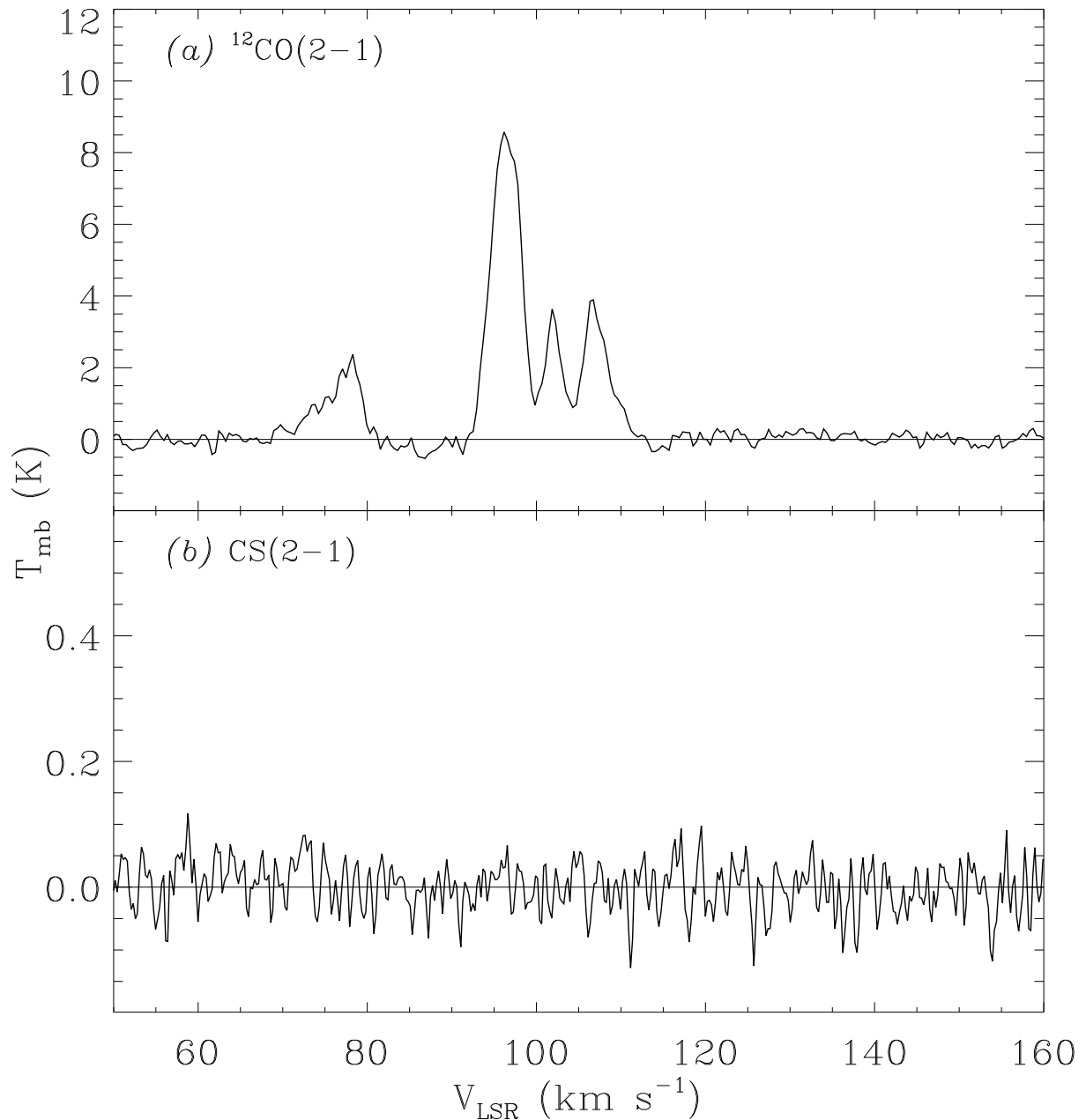


Fig. 2.— Spectra of (a)  $^{12}\text{CO}(2 \rightarrow 1)$  and (b) CS( $2 \rightarrow 1$ ) emission from the brightest part of the radio shell of 3C 391. Each spectrum is the average of spectra within  $21''$  of relative position  $(-130'', +90'')$ .

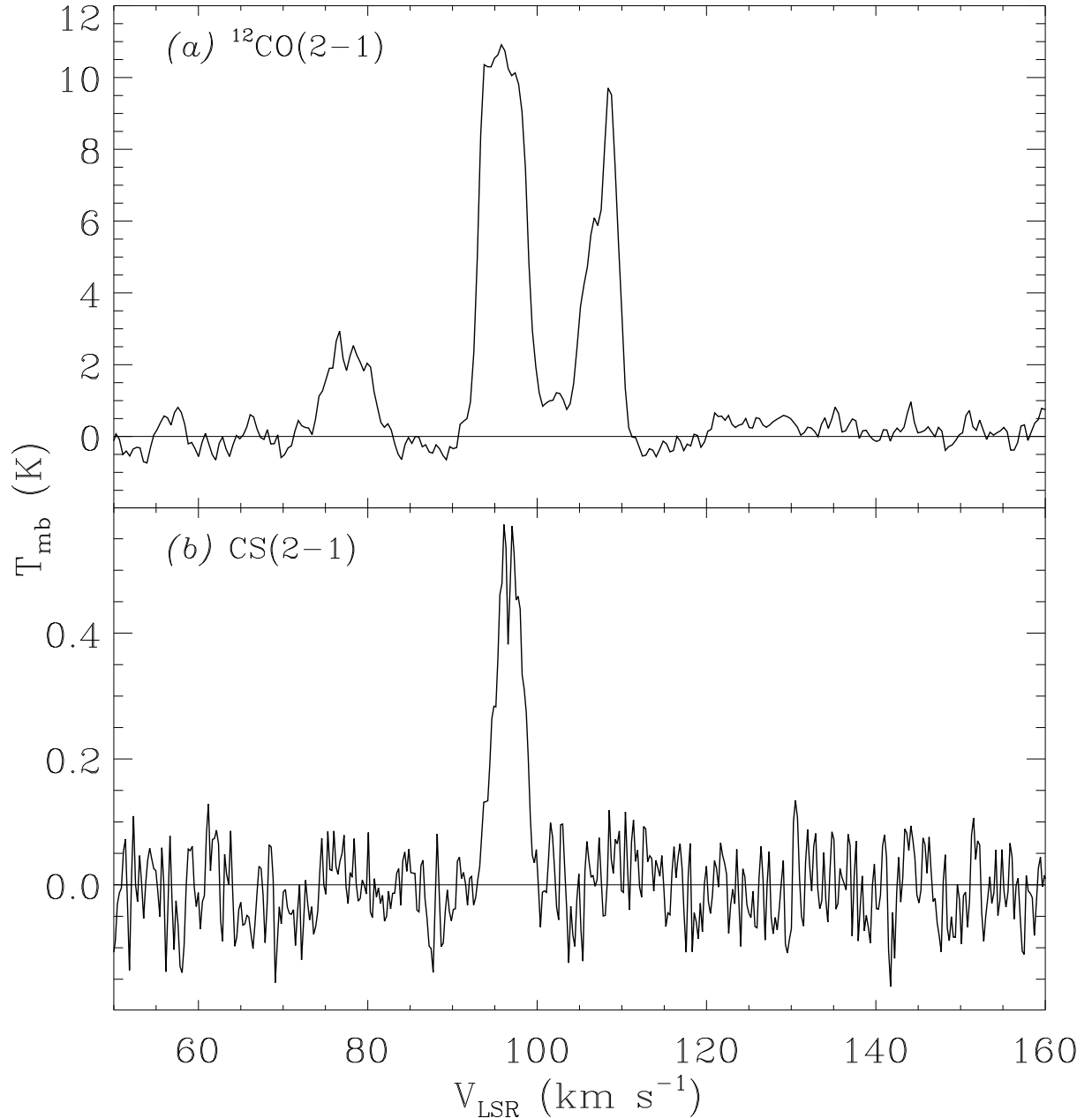
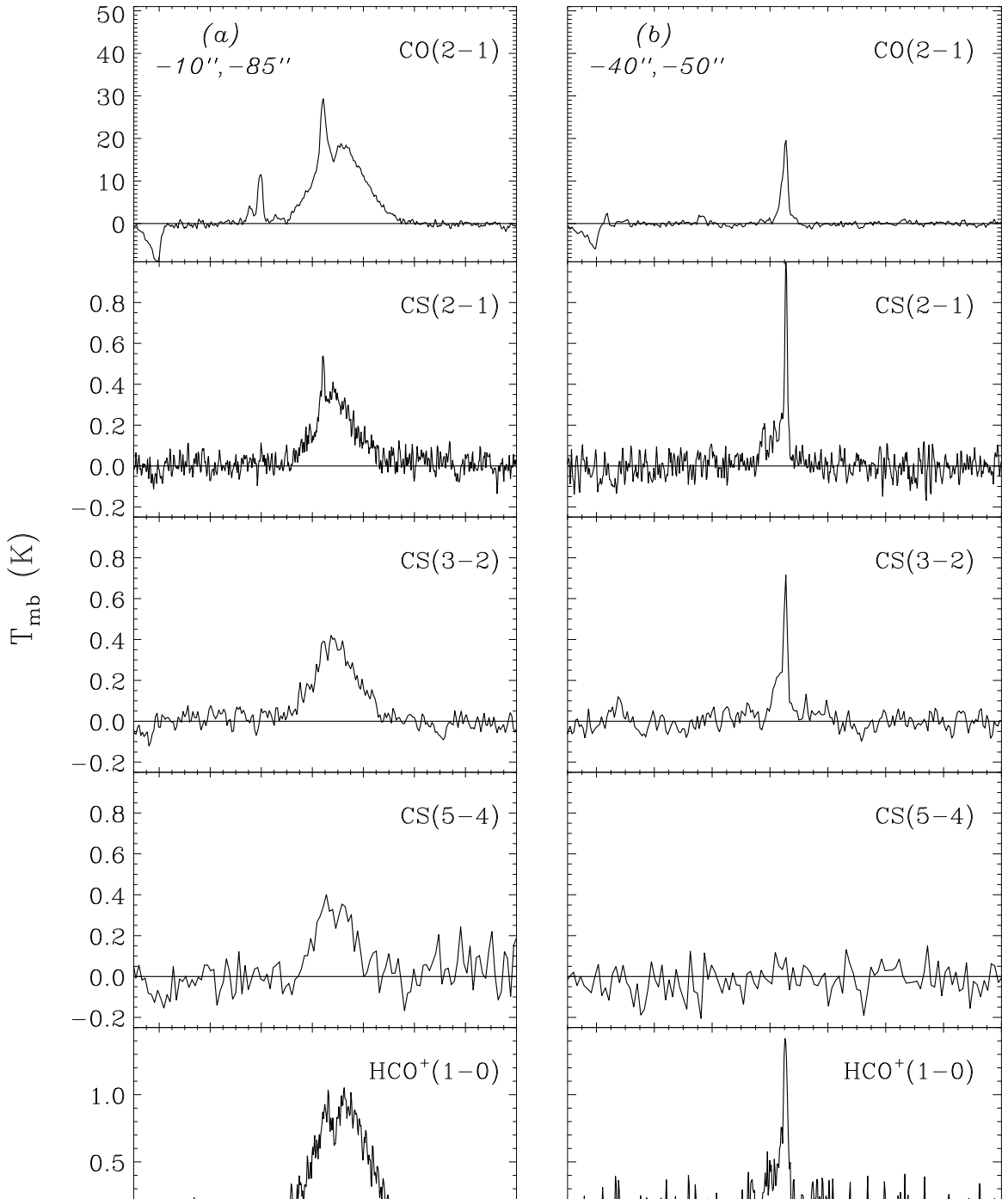


Fig. 3.— Spectra of (a)  $^{12}\text{CO}(2 \rightarrow 1)$  and (b)  $\text{CS}(2 \rightarrow 1)$  emission a relatively bright clump in the ambient gas in the parent molecular cloud. Each spectrum is the average of spectra within  $21''$  of relative position  $(-130'', +240'')$ .

Fig. 4.— Spectra of the 3C 391 shocked molecular clump. The spectra in the right-hand panel (*a*) are toward the peak of the wide-line emission of this clump, at relative position  $(-40'', -50''). The spectra on the right-hand panel (*b*) are toward the peak of narrow-line emission from this clump, at relative position  $(-10'', -85'')$ . Note that the wide emission lines are much brighter in the high-excitation  $\text{CS}(5 \rightarrow 4)$  line, compared with the narrow-line region. The spectra of the narrow-line region are similar to those of the parent molecular cloud in width and relative line brightnesses.$



measure its physical properties in more detail in the discussion below.

The shape of the spectral lines changes rather abruptly in the shocked clump, and these line shape variations offer further clues to the nature of the emitting region. The  $^{12}\text{CO}(2 \rightarrow 1)$  line profiles on a  $10'' \times 10''$  grid are shown in Figure 5. Both the wide and narrow components of the spectral lines are bright in this region, but their distributions are significantly different. We separated the wide and narrow components from each spectrum, in order to show their distributions separately. For the narrow component, we subtracted a linear baseline fitted in a small spectral window within  $2 \text{ km s}^{-1}$  of the narrow-line peak; this ‘baseline’ includes the wide component at the velocity of the narrow component peak. For the wide component, we calculated the total line integral over 85 to 130  $\text{km s}^{-1}$  and subtracted the narrow component line integral. A map of the wide and narrow components of the  $\text{CS}(2 \rightarrow 1)$  lines is shown in Figure 6. The narrow component peaks to the southeast and the wide component to the northwest of the OH maser position, which is shown with an asterisk. The  $^{12}\text{CO}(2 \rightarrow 1)$  results are similar, but with a more extended narrow-line region. The  $\text{CS}(5 \rightarrow 4)$  line profiles show *only* the wide component, and the  $\text{CS}(3 \rightarrow 2)$  profiles are intermediate between the higher and lower CS transitions.

Both the narrow and wide components are clearly related to the SN-MC interaction because they both peak in the same region, and we are evidently resolving regions of very distinct physical conditions. However, the exact relationship between the wide and narrow components is not clear. The narrow component could be due to pre-shock gas, a hypothesis motivated by the fact that the dense clump in the parent molecular cloud has the same spectral lines in about the same proportions. Alternatively, the narrow component could be due to molecules that have reformed in gas that has cooled behind a fully dissociative shock. This second hypothesis is motivated by the fact that the narrow component is spatially near the wide component, there are infrared lines indicating a dissociative shock, and the velocity of the narrow component closely matches that of the shock-excited 1720 MHz OH maser. However, the present observations do not clearly distinguish between these hypotheses. Indeed, the cold region far behind a dissociative shock *should* be difficult to discern from pre-shock gas.

## 5. Overall distribution of shocked molecular gas

The region shown in Figures 5 and 6 covers only a small part of the whole supernova remnant. In particular, it does not include the location where one might expect the strongest impact of the shock on the parent molecular cloud—specifically, the ridge of very bright radio emission that runs precisely along the edge of the molecular cloud. The  $^{12}\text{CO}(2 \rightarrow 1)$  and  $\text{CS}(2 \rightarrow 1)$  spectra of the bright radio ridge are shown in Figure 2. There is no trace of the wide emission line that characterized the shocked clump in Figure 4. The  $^{12}\text{CO}(2 \rightarrow 1)$  line profile at the radio shell splits into three components, with widths (FWHM) of 2 to 4  $\text{km s}^{-1}$ . If there is emission from a wide spectral component, then it must be more than 40 times weaker at the radio shell than toward the shocked clump. Further, there is no CS or  $\text{HCO}^+$  emission detected toward the radio

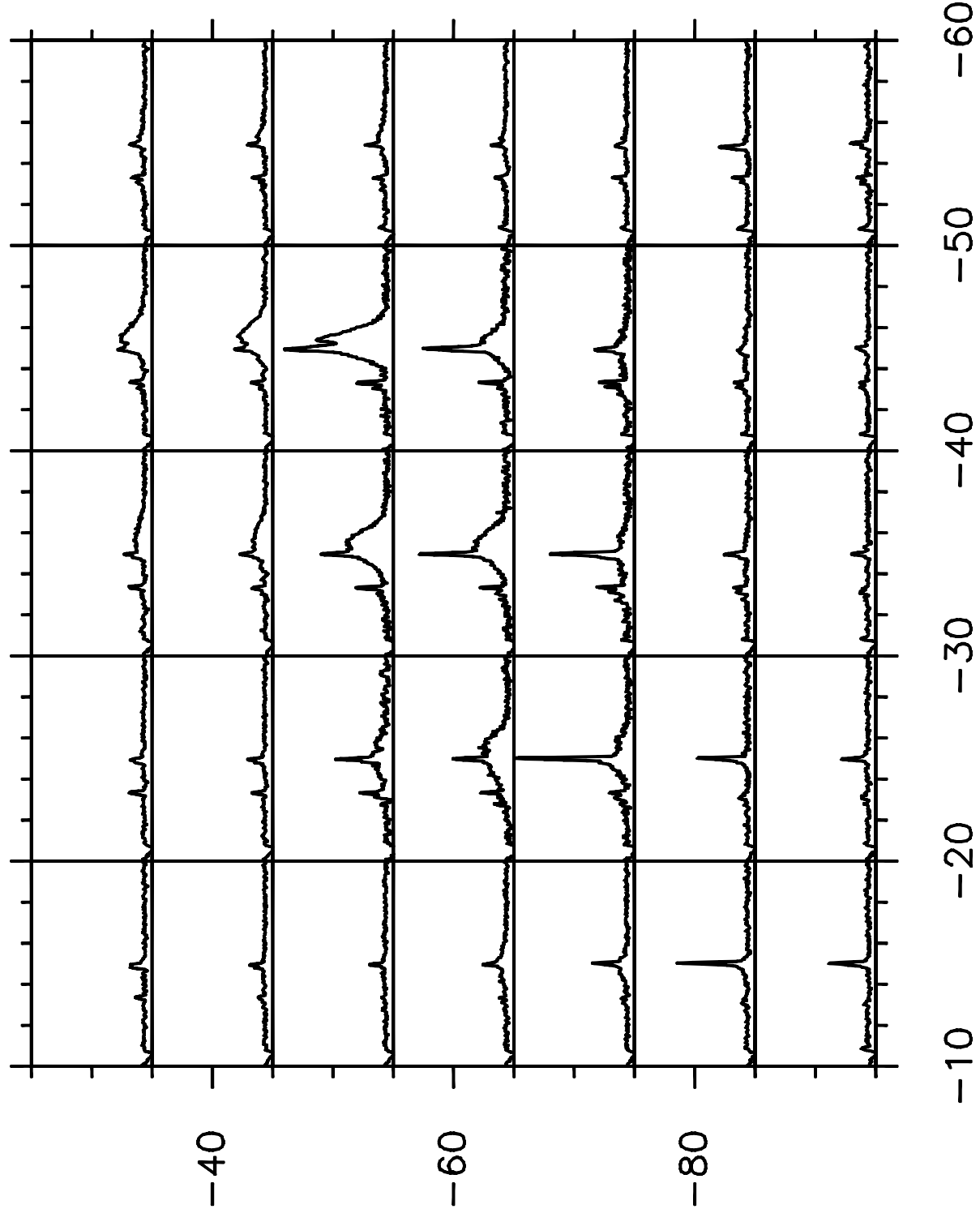


Fig. 5.— Grid of  $^{12}\text{CO}(2 \rightarrow 1)$  spectra near Maser 1. The spacing between spectra is 10'', the velocity scale in each box is from 30 to 180  $\text{km s}^{-1}$ , and the main beam brightness temperature in each box ranges from -4 to 62 K. The line profile changes rapidly from position to position. The narrow component of the line profile is the pre-shock gas, while the broad component (with a width of 20  $\text{km s}^{-1}$ ) is the shocked gas.

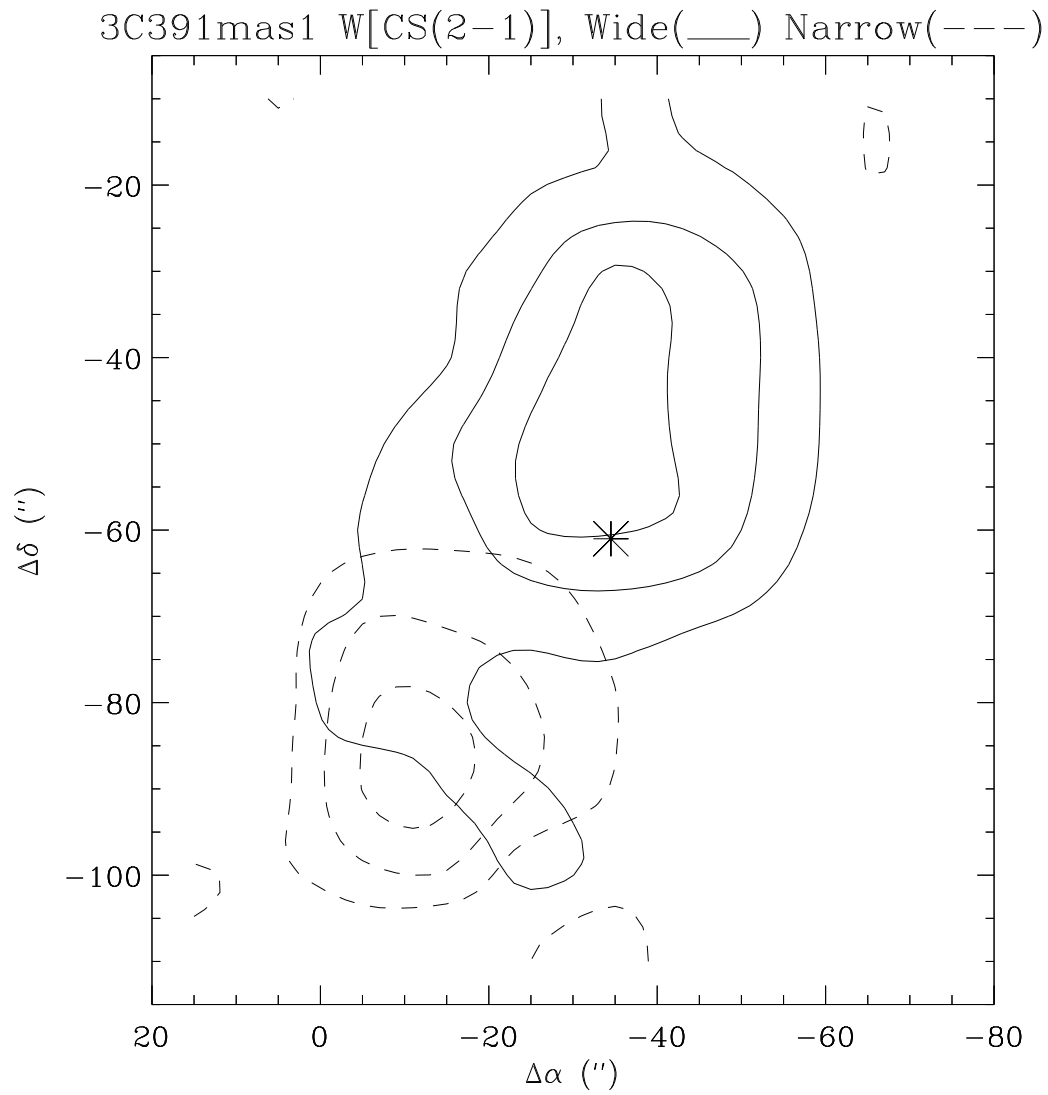


Fig. 6.— A small map showing separately the brightnesses of the wide (solid contours) and narrow (dashed contours) components of the CS( $2 \rightarrow 1$ ) lines for the Maser 1 clump. The position of the OH maser is indicated by an asterisk.

shell; *neither* the wide nor narrow components are present.

In order to determine whether the spectrum toward the radio shell is ‘normal’, and to illustrate the properties of spectral lines from the parent molecular cloud, we show the spectrum of a bright clump from the parent molecular cloud in Figure 3. This clump was identified as a peak in the CS( $2 \rightarrow 1$ ) map, and its CO lines are some of the widest in the parent molecular cloud. The broadening of the CO lines is almost certainly due to saturation: the CO lines are very optically thick. The CO component at  $96 \text{ km s}^{-1}$  is the one that actually peaks at this position, and is the only one in the CS spectrum. The line brightnesses and widths are summarized in Table 2. Comparing the molecular spectra of the radio shell, the parent molecular cloud, and other molecular clouds from the galactic plane (Clemens et al. 1986), we see no evidence that there is any interaction between the molecular gas and the supernova remnant, despite the strongly suggestive arrangement of the radio shell exactly along the face of the molecular cloud.

It is possible, however, that the interaction between the shock and the molecular cloud leaves little or no trace in the observed molecular lines, and the shocked clump 3C 391:cs is a rare exception. We looked for more subtle indications of interaction by making maps in each of the main velocity components of the molecular lines. Note that only toward the shocked clump is there clear evidence for a very wide spectral line. Everywhere else, the  $^{12}\text{CO}(2 \rightarrow 1)$  and CS( $2 \rightarrow 1$ ) lines (where detected) consist of a sum of relatively narrow, Gaussian-shaped components. There are 3 distinct velocity components of the  $^{12}\text{CO}(2 \rightarrow 1)$  and CS( $2 \rightarrow 1$ ) lines between  $90$  and  $120 \text{ km s}^{-1}$  that appear in at least part of the 3C 391 region. One of the spectral components (whose map is shown in Figure 1) is the bulk of the ambient molecular cloud, which dominates to the northwest of the remnant. Maps of the other two components are shown in Figures 7 and 8.

Inspecting these maps, there is some evidence for a widespread interaction between 3C 391 and its parent cloud, roughly following the entire hemisphere of the remnant facing the molecular cloud. There is a long, nearly straight filament in the  $109 \text{ km s}^{-1}$  map (Fig. 7) that runs roughly along the inside of the northeastern part of the bright radio shell, all the way to the southeastern extent of the bright radio emission. A spur from this filament includes the position of the second OH maser (Frail et al. 1996), and the velocity and width of the CO, CS, and OH lines are in good agreement. Based on the unusual morphology, running along the edge of the non-thermal radio shell, and the agreement in position and velocity with a shock-excited OH maser, we suspect that the filament is related to the SN-MC interaction, even though the width of the spectral lines in the filament is similar to that of the ambient gas.

Figure 8 shows the distribution of gas with velocities near  $105 \text{ km s}^{-1}$ . This is the velocity at which the narrow component of the clump 3C 391:cs peaks, and it contains part of the wide component as well. The map is dominated by a bright peak at the position of 3C 391:cs, but it has secondary peaks in the parent molecular cloud as well as some diffuse emission connecting the parent molecular cloud to 3C 391:cs. The diffuse emission has a rough correspondence with the southwestern part of radio shell, and it contains—both in position and central velocity—the

Fig. 7.— Map of the  $^{12}\text{CO}(2 \rightarrow 1)$  line integrated over the velocity range 108 to 110  $\text{km s}^{-1}$ .

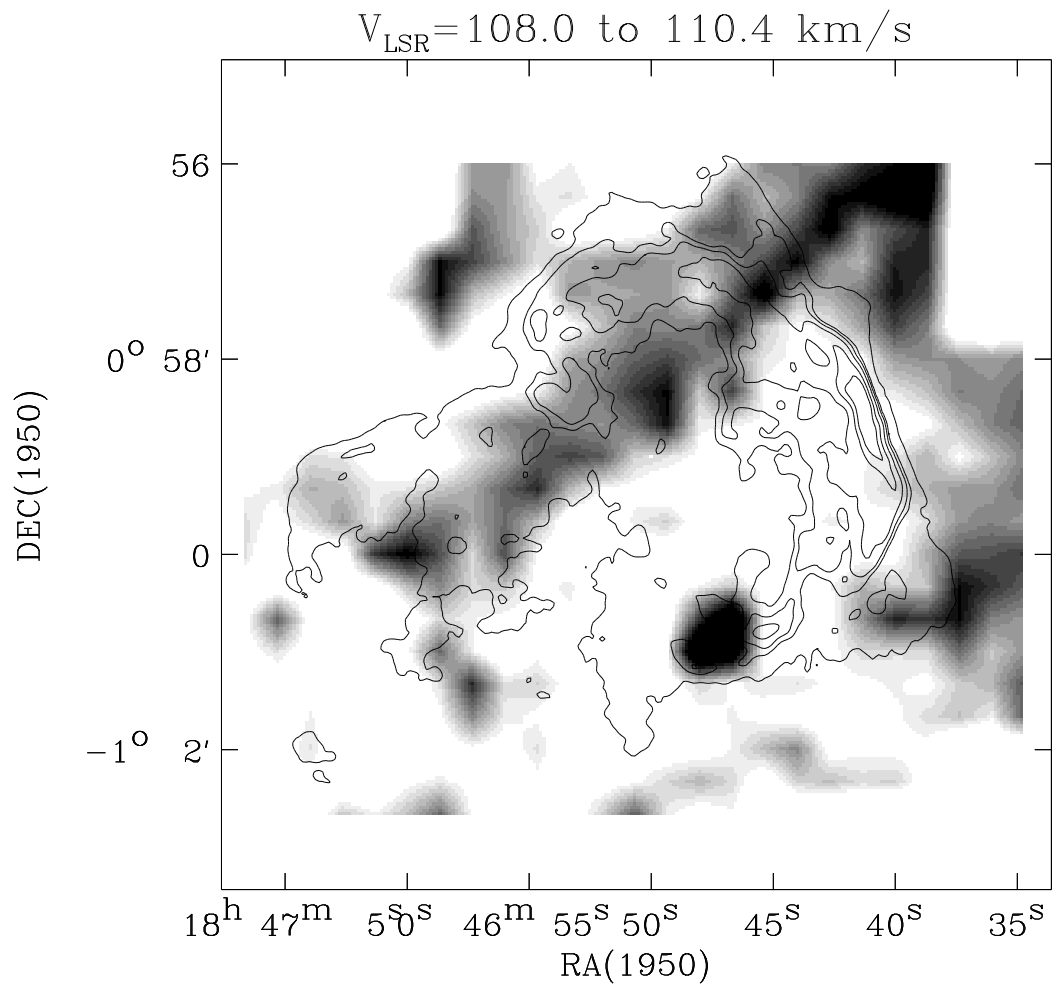
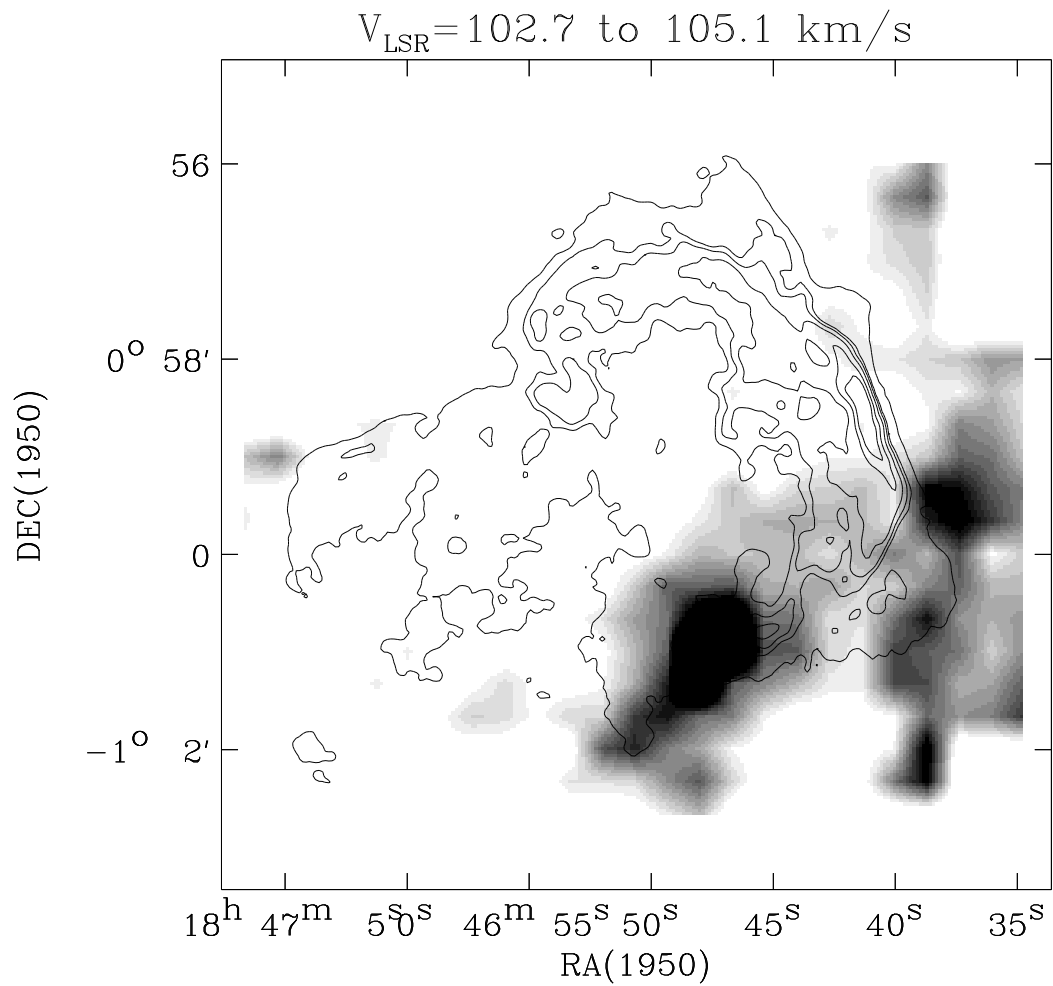


Fig. 8.— Map of the  $^{12}\text{CO}(2 \rightarrow 1)$  line integrated over the velocity range 104 to 106  $\text{km s}^{-1}$ .



region with the strongest SN-MC interaction; therefore, this emission may also be related to the SN-MC interaction. The overall distribution of the molecular gas in Figs. 7 and 8, could be due to a hemisphere of displaced gas, with the open end pointing away from the parent molecular cloud. In this picture, 3C 391 is a ‘CO-shell’ remnant—the first of its kind. The ‘shell’, however, is neither spatially complete nor kinematically coherent, which is not surprising considering that the ambient molecular cloud contains a great deal of structure.

## 6. Excitation of the Molecular Gas

### 6.1. Three-line analysis of the CS excitation

Using the three observed transitions of CS, we can constrain the physical conditions in the shocked gas. We compared the line brightnesses to Large Velocity Gradient (LVG) models for a range of gas temperature,  $T$ , CS column density,  $N(\text{CS})$ , and gas density,  $n(\text{H}_2)$ . We can reject the possibility that the observed lines are in Local Thermal Equilibrium (LTE), because the observed CS line ratios imply kinetic temperatures even lower than the observed CO brightness temperatures; that is, the excitation of CS must be sub-thermal. This is not surprising, because the critical density for collisional de-excitation of the  $\text{CS}(5 \rightarrow 4)$  line is very large:  $n_c \simeq 8 \times 10^6 \text{ cm}^{-3}$ . So far, we have only considered excitation by collisions with  $\text{H}_2$  molecules, which is probably sufficient for the ambient cloud. For the shocked gas, some excitation by collisions with atomic H or even electrons is possible if the  $\text{H}_2$  formation is incomplete or the ionizing photon field is strong; in this case, our  $n(\text{H}_2)$  refers to a composite of the  $\text{H}_2$ , H, and electron densities responsible for the CS excitation. It is quite likely that the shocked gas is partially dissociated, so that H is the dominant collision partner there, as was found in W 51C (Koo & Moon 1997b). Based on previous work in interpreting similar CS observations of diffuse clouds (Reach et al. 1994), dipole selection rules mean electrons will be of relatively little importance except for  $1 \rightarrow 0$  transitions, such as the bright  $\text{HCO}^+(1 \rightarrow 0)$  lines; the positive charge of  $\text{HCO}^+$  also means electrons are likely to be important in its excitation.

Model parameters consistent with the observations for two positions are illustrated in Figure 9. The first position is the strongly-shocked clump—wide spectral component only—for which the spectra were shown in Figure 4). The second position is a dense clump in the parent molecular cloud, well *outside* the remnant. Models were calculated on a grid of  $N(\text{CS})$ ,  $n(\text{H}_2)$ , and  $T$ . The temperature cannot be determined separately from the volume density for the ambient gas, because only 2 lines were detected. We assume a temperature of 20 K for the clump in the parent molecular cloud. This temperature is consistent with the lower limit set by the observed brightness temperature of the  $^{12}\text{CO}(2 \rightarrow 1)$  line, and it is in between the 10–15 K inferred from  $\text{NH}_3$  and CS observations of dark clouds (Benson & Myers 1989; Snell, Langer, & Frerking 1982) and higher temperatures found in star-forming cores from  $\text{H}_2\text{CO}$  observations (Mangum & Wootten 1997). For reference, we note that in LTE the observed CS line ratio yields an excitation

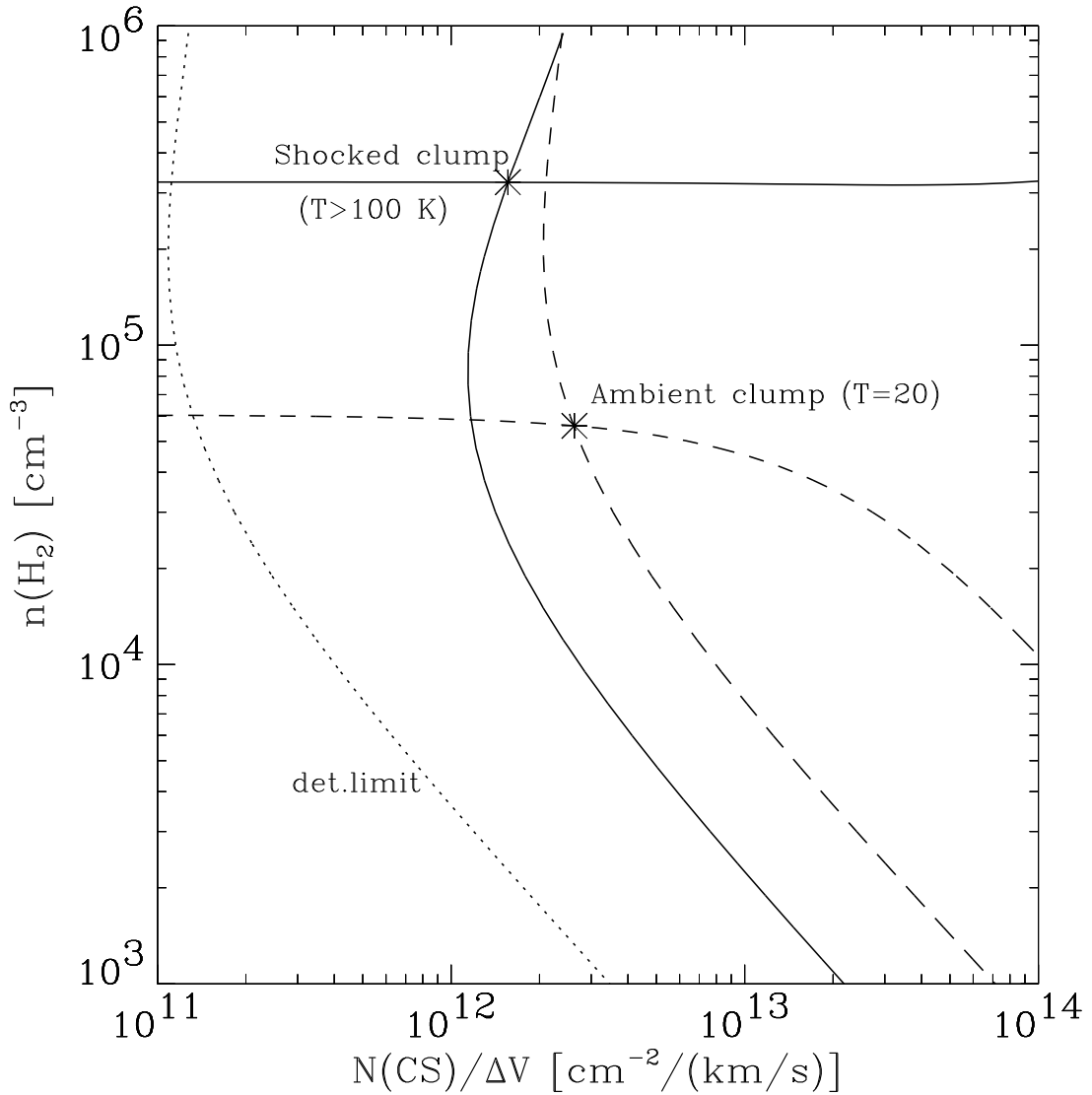


Fig. 9.— Excitation diagram for CS, showing the values of H<sub>2</sub> volume density and CS column density of LVG calculations that satisfy the following constraints. The upper asterisk shows the best model for the shocked clump. The two solid curves passing through this asterisk show separately the constraints imposed by the  $5 \rightarrow 4$  to  $2 \rightarrow 1$  ratio (horizontal line) and the brightness of the  $3 \rightarrow 2$  line (more nearly vertical curve); models are for a kinetic temperature of 100 K. Similarly, the lower asterisk and curves through it show the constraints for the ambient clump in the parent molecular cloud, with the nearly horizontal curve being imposed by the  $3 \rightarrow 2$  to  $2 \rightarrow 1$  ratio and the vertical curve by the brightness of the  $2 \rightarrow 1$  line; models are for a temperature of 20 K. Finally, the dotted curve near the left edge of the plot shows the detection limit for the CS( $2 \rightarrow 1$ ) line, which applies to the radio ridge region.

temperature of only 3.7 K, which is clearly lower than the gas temperature. The contours of constant  $3 \rightarrow 2/2 \rightarrow 1$  ratio and  $2 \rightarrow 1$  brightness for the ambient clump are shown in Figure 9. These constraints intersect at a volume density of  $6 \times 10^4 \text{ cm}^{-3}$  and a CS column density of  $9 \times 10^{12} \text{ cm}^{-2}$ . Assuming we are observing a uniform clump with depth equal to transverse size, then the abundance of CS relative to  $\text{H}_2$  is  $2 \times 10^{-10}$ . We take these values to characterize the densest clumps in the parent cloud. There are of course wide density variations in the molecular cloud. The CS( $3 \rightarrow 2$ ) emitting regions have densities  $> 10^4 \text{ cm}^{-3}$ ; they are detected over most of the ambient cloud but probably do not fill its volume.

## 6.2. Physical parameters of the shocked gas

For the shocked gas, we found that low-temperature models are not able to produce the CS( $5 \rightarrow 4$ ) emission in the observed amounts, even at very high densities. A lower limit to the gas temperature is the observed brightness temperature of the  $^{12}\text{CO}(2 \rightarrow 1)$  line:  $T_k > 18 \text{ K}$ . In the high-density limit (LTE), the observed line ratios yield  $T_k = 7\text{--}13 \text{ K}$ , depending on which pair of lines is used; this LTE solution is inconsistent with the observed brightness temperature. There is a family of LVG solutions that can approximately match the observed line brightnesses. First, there is a lower limit for the temperature of the shocked gas is given by the lowest temperature that can produce the observed ratio of  $5 \rightarrow 4/2 \rightarrow 1$  brightness:  $T_k > 40 \text{ K}$ . Within the range 40–100 K, the models that match the observed  $5 \rightarrow 4/2 \rightarrow 1$  ratio require densities in the range of  $1\text{--}0.3 \times 10^6 \text{ cm}^{-3}$ . The highest temperature that we considered in the LVG analysis, 100 K, gives a rough match to all three CS lines, though higher temperatures will probably also work. None of the models match all three lines, although agreement improves as the temperature increases. The excitation of the shocked gas is also constrained by relative  $^{12}\text{CO}(2 \rightarrow 1)$  line brightness compared to  $^{12}\text{CO}(1 \rightarrow 0)$  from Wilner et al. (1998). There is no wide component detected in the  $^{12}\text{CO}(1 \rightarrow 0)$  line, but we can limit it to  $T_b(1 \rightarrow 0) < 1.5 \text{ K}$  within the beam of the 12-meter telescope. The relative filling factor of the wide component in the 12-meter beam  $\sim 0.3$  based on our map, so we can limit the ratio of  $1 \rightarrow 0/2 \rightarrow 1 < .3$ . The CO lines, unlike CS, are likely to be thermalized because of the lower dipole moment of the former molecule; using LTE, the CO line ratio implies  $T_k > 50$ . We conclude that the shocked clump is both significantly more *hot* and *dense* than the densest clumps in the parent cloud, while the narrow-line emitting region of the shocked clump is similar to a dense clump in the parent molecular cloud. Therefore, there is an abrupt change in the physical properties of the molecular-line emitting gas within 3C 391:cs.

The column density of CS is well determined in the shocked gas, because we directly observed the column density of CS molecules in levels  $J = 2, 3$ , and  $5$ , which include the most-populated levels. For the shocked gas,  $N(\text{CS}) = 3 \times 10^{13} \text{ cm}^{-2}$ . If the wide-line emitting region is uniform and spherical, then the column density of the collision partner of CS, presumably  $\text{H}_2$  but including  $\text{H I}$ , is  $N \simeq 10\text{--}6 \times 10^{23} \text{ cm}^{-2}$ , and the CS abundance in the wide-line emitting region is  $1\text{--}5 \times 10^{-11}$  for temperatures 40–100 K. For this calculation and those that follow, we assume a distance

to 3C 391 of 9 kpc, which is based on the comparison of H I 21-cm emission and absorption line profiles (Radakrishnan et al. 1972) and the H<sub>2</sub>CO absorption line at 96 km s<sup>-1</sup> (Downes et al. 1980); our adopted distance is consistent with that adopted by others for this remnant (Reynolds & Moffett 1993). This CS abundance is about an order of magnitude *lower* than in the dense clump in the parent molecular cloud, suggesting that the CS was dissociated and has not completely reformed behind the shock. However, it is possible that the emitting region does not fill the beam, even though the emitting region is clearly resolved. For a fast, dissociative shock, the thickness from the shock front to where the gas has cooled to 100 K is only predicted to be of order 0.03 pc (Hollenbach & McKee 1989), compared to the 0.6 pc extent of the region where we observed the wide emission lines. The CS abundance in the shocked clump could therefore be as high as that of the dense clump in the parent molecular cloud, and the CS molecules could be nearly completely reformed behind the shock—or never dissociated at all. If this is true, then the wide-line emitting region would comprise a network of relatively thin shock fronts that could be revealed in higher-resolution images.

The chemistry of the shocked gas is apparently not significantly different from that of the parent molecular cloud, at least for the molecules that we have observed. While all molecular abundances appear low relative to the H<sub>2</sub> column inferred from the CS excitation, the relative abundances between the molecules we actually detected is very similar to that of dense, quiescent molecular gas. The relative abundances relative are nearly independent of the kinetic temperature or density. We find CS/CO $\simeq (1 \pm 0.3) \times 10^{-4}$ , and HCO<sup>+</sup>/CS $\sim 0.5$ . These abundances are very similar both to those found for the shocked gas in IC 443 (Ziurys, Snell, & Dickman 1989; van Dishoeck et al. 1993) and W 51C (Koo & Moon 1997b), and to those of quiescent gas in TMC 1 and the Orion ridge (Irvine et al. 1987). The fact that our abundances are all low relative to H<sub>2</sub> (as inferred from the excitation of CS) could be due to a combination of (1) the emitting region is structured on smaller scales, (2) we have missed some of the molecules because we only observed a limited number of transitions, and (3) there is a range of physical conditions on the line of sight so that different lines come from different regions. Assuming that atomic H is the dominant collision partner, rather than H<sub>2</sub>, only helps by about a factor of about 2, because 2 H atoms are unlikely to be much more effective than one H<sub>2</sub> molecule. The discrepancy between excitation and abundance is not unique to shocked gas; this is a more general problem in understanding the excitation of molecular gas (see, *e.g.*, Falgarone et al. 1998). If ambient molecular gas is already highly structured on very small scales, then it would not be surprising for the post-shock to be also highly structured.

### 6.3. Dynamics of the shocked gas

The velocity of the shocks that compressed and heated 3C 391:cs can be estimated in several ways. The width of the wide spectral component probably gives a lower limit to the shock velocity,  $v_s > 20$  km s<sup>-1</sup>, because it is a one-dimensional projection onto the line of sight. Furthermore the

gas might not be detected along the entire range of velocities between the pre-shock and post-shock gas, as it may be dissociated part of the time. Another estimate is obtained by comparison with the CO emission predicted for magnetohydrodynamic shocks by Draine & Roberge (1984): the  $^{12}\text{CO}(2 \rightarrow 1)$  line brightness we observed from the wide-line clump ( $\sim 5 \times 10^{-6} \text{ erg s}^{-1} \text{ cm}^{-2} \text{ sr}^{-1}$ ) is consistent with models for a pre-shock density of  $10^4$ – $10^5 \text{ cm}^{-3}$  and a range of shock velocities  $v_s \simeq 10$ – $50 \text{ km s}^{-1}$ . This is consistent with the observed linewidth, if we are observing shock fronts with a range of orientations relative to our line of sight. The location of the 3C 391:cs near the edge of the remnant suggests that the shock would be perpendicular to the line of sight, favoring higher values of  $V_s$ . This range of shock velocities is near the transition between dissociative (J) and non-dissociative (C) shocks. In W 51C, Koo & Moon (1997b) concluded that the shock was dissociative, and the CO molecules have re-formed while the H remains largely atomic. In contrast, we suspect that the wide emission lines in 3C 391:cs are from a shock that is only partially dissociative. This is consistent with the fact that the pre-shock density is substantially higher for 3C 391:cs than was estimated for W 51C.

A simple estimate of the ram pressure of the 3C 391 blast wave (energy per unit volume, assuming adiabatic expansion) suggests that it drive shocks with  $n_0 v_s^2 \sim 3 \times 10^5 E_{51}$ , where  $n_0$  is the pre-shock density in  $\text{cm}^{-3}$ ,  $v_s$  is the shock velocity in  $\text{km s}^{-1}$ , and  $E_{51}$  is the SN energy in  $10^{51} \text{ erg}$ . The pressure we infer from comparing models to the CO brightness is two orders of magnitude higher than that for the blast wave. The same conclusion was reached from interpretation of the bright [O I] 63  $\mu\text{m}$  lines from this remnant and W 44 (Reach & Rho 1996). Moorhouse et al. (1991) also inferred surprisingly high pressure ( $\sim 25$  times) from a molecular hydrogen observation of IC 443. The pressure of a J-shock that produces the observed [O I] brightness is comparable to the pressure of a C-shock that produces the observed CO brightness. We can consider a few possible explanations for why the spectral diagnostics yield such high pressures. The first possibility is that the pressure is higher due to reflected shocks. When a blast wave hits a high density structure, the shock splits into reflected and transmitted shocks. For a density ratio  $\sim 10^3$  between the cloud and the inter-cloud medium, the pressure is enhanced a factor of several in plane-parallel, uniform-density models (Borkowski, Blondin, & Sarazin 1992; Hester, Raymond, & Blair 1994). While a reflected shock does not appear to be fully sufficient, a model accounting for similar physical processes and the specific conditions for 3C 391 (a globally adiabatic remnant impacting a giant molecular cloud) might yield higher pressures.

Another scenario is gravitational binding of the clumps, after compression by the strong shock. Assuming the dominant collision partner of CS is  $\text{H}_2$ , and assuming the emitting region is a uniform sphere, the mass of 3C 391:cs is of order  $10^4 M_\odot$ . The gravitational pressure  $\rho v_{esc}^2$ , estimated using the escape velocity at the edge (0.6 pc radius) is of order  $10^{-7} \text{ dyne cm}^{-2}$ , which is comparable to that inferred from the molecular and [O I] line brightnesses. There is some evidence (from the apparently depressed abundances of all species relative to  $\text{H}_2$ ) that the emitting region is *not* uniform and the total mass could be 2 orders of magnitude lower. However, taken at face value, a uniform emitting region would have a very significant self-gravity. Therefore, we

could be observing in 3C 391:cs the triggering of star formation. Star formation could not have occurred yet, since the free-fall time is longer than the remnant age. We estimate that the shock hit the dense clump about 400 yr ago, based on the distance of the clump behind the the radio continuum shell. A similar scenario was first considered by Elmegreen & Lada (1977), where shock waves trigger star formation by compressing adjacent molecular clouds. In the case of 3C 391, the present configuration appears consistent with a single explosion near the edge of a molecular cloud. The bright radio continuum shell and the CO shell would correspond to the the layer considered by Elmegreen & Lada. This entire layer may not become gravitationally unstable from the action of a single remnant, but 3C 391:cs could collapse separately to form one or several stars.

## 7. Implications for molecular shocks in other supernova remnants

Given the high brightness temperature and line-width of the emission from the strongly-shocked clumps in 3C 391, IC 443, and W 51C, why hasn't shocked gas been observed in other supernova remnants? First, the strongly-shocked gas occupies a very small region ( $< 0.6$  pc). Therefore, it will be either beam-diluted or easily missed in low-resolution or incompletely-sampled maps. Second, detection of the broad line requires a wide bandwidth and flat baseline, both of which were possible in good observing conditions and using modern correlators. A third reason that other shocked molecular clouds like those in 3C 391 and IC443 have not been detected is that they are much less prominent in lower-excitation lines like  $^{12}\text{CO}(1 \rightarrow 0)$ . The shocked gas is comparable to pre-shock gas in  $^{12}\text{CO}(2 \rightarrow 1)$  and  $\text{CS}(2 \rightarrow 1)$  emission and dominates for higher excitation transitions. Fourth, there is often confusion in the line profiles due to absorption by molecular gas both from the parent molecular clouds and clouds along the line of sight. In the shown spectra in Figure 4, there are dips that could be self-absorptions in the  $\text{HCO}^+(1 \rightarrow 0)$  and  $^{12}\text{CO}(2 \rightarrow 1)$  lines. However, we were able to obtain a  $^{13}\text{CO}(1 \rightarrow 0)$  spectrum at this position that showed that the cold gas peaks at the same velocity of the narrow component—not at the velocity of the dips in the spectra. The *lack* of self-absorption is one of the main reasons why we can clearly see the shocked gas from 3C 391. For comparison with W 44, the complicated line profiles of the shocked gas left some doubt as to whether the emission is broad or just multiple components (DeNoyer 1983); however, the dips in the  $^{12}\text{CO}(1 \rightarrow 0)$  profile are correlated to peaks in the  $^{13}\text{CO}$  profile (Seta 1996), showing that they are self absorption. We found that this relationship occurs in detail over several areas of the supernova remnants W 44 and W 28, and will report these results in a later paper. The more extended, narrow-line emission that we suggested is a ‘CO shell’ for 3C 391 is not clearly distinct from ambient molecular gas, and we have relied on morphological agreement with the radio shell as well as position and velocity agreement with the shock-excited OH masers. Wide- and narrow-line shocked regions, and narrow-line ambient regions are expected to coexist, until such a time as the shock has completely passed through the all the dense clumps, leading to complicated line profiles. These factors are likely to be true for the other remnants interacting with molecular clouds, and we expect more detections of similar objects in the future.

## 8. Conclusions

We observed the entire supernova remnant 3C 391 in millimeter lines of CS, CO, and  $\text{HCO}^+$ . The lower-excitation lines reveal a giant molecular cloud to the northwest of the remnant, explaining the ‘break-out’ morphology of the radio emission. The interactions between the blast wave and a very dense molecular clump was found within a small ( $50''$ ) region that we call 3C 391:cs. A wide component (FWHM  $25 \text{ km s}^{-1}$ ) and a narrow component (FWHM  $2 \text{ km s}^{-1}$ ) both peak at 3C 391:cs, which is coincident with an OH 1720 MHz maser. The excitation of the wide molecular lines requires both high gas temperature ( $> 100 \text{ K}$ ) and density ( $\sim 3 \times 10^5 \text{ cm}^{-3}$ ). The narrow-line region require somewhat lower density and are consistent with much lower ( $\sim 20 \text{ K}$ ) temperatures. We identified a clump in the parent molecular cloud with properties similar to the narrow-line region. Therefore, the 3C 391:cs clump was similar to the highest-density clumps in the parent molecular cloud, and it is currently being shocked. The brightness of the wide  $^{12}\text{CO}(2 \rightarrow 1)$  line from 3C 391:cs is consistent with C-type molecular shocks with  $10^4 < n_0 < 10^5 \text{ cm}^{-3}$  and  $10 < v_s < 50 \text{ km s}^{-1}$ , or J-type shocks with  $n_0 \sim 10^3$  and  $v_s \sim 100 \text{ km s}^{-1}$ . The pressure in the shocked clump is much higher than the estimated ram pressure of the remnant, possibly because of its self-gravity. If so, this clump is a likely site of triggered star formation. A widespread interaction of 3C 391 with molecular gas is evidenced by the distribution of CO and CS lines with central velocities offset from that of the parent cloud by 10 to  $15 \text{ km s}^{-1}$ ; these velocities correspond to those of the two OH masers. The interaction comprises nearly an entire hemisphere of the remnant, making 3C 391 a ‘CO shell’ remnant.

**Acknowledgment** We thank Hans Ungerechts at IRAM for helping us get started on the IRAM telescope and David Wilner and Steve Reynolds for sharing early results of their observations. WTR thanks the Commissariat d’Energie Atomique, in Saclay, France for hospitality and computing power during part of the data analysis. We thank Bon-Chul Koo for his comments and support.

Table 1. Observed spectral lines and Telescope parameters

transition	frequency (GHz)	$T_{sys}^a$ (K)	$\eta_{mb}$	beam ( $''$ )	$\delta v^b$ ( $km\ s^{-1}$ )	$\Delta v^c$ ( $km\ s^{-1}$ )
$HCO^+(1 \rightarrow 0)$	89.1885	310	0.82	27	0.22	430
CS( $2 \rightarrow 1$ )	98.9798	250	0.76	24	0.24	430
CS( $3 \rightarrow 2$ )	146.9690	240	0.58	16	0.65	290
CS( $5 \rightarrow 4$ )	244.9356	490	0.43	10	1.2	310
CO( $2 \rightarrow 1$ )	230.5380	720	0.45	10	1.3	330

<sup>a</sup>typical system temperature for observations presented in this paper

<sup>b</sup>velocity resolution

<sup>c</sup>velocity coverage

Table 2. Measured properties of spectral lines<sup>a</sup>

transition	$T_{mb}$ (K)	$V_{LSR}$ ( km s <sup>-1</sup> )	$\Delta V$ (FWHM) ( km s <sup>-1</sup> )
wide-line position in shocked clump ( $-40''$ , $-50''$ ) <sup>b</sup>			
HCO <sup>+</sup> (1 $\rightarrow$ 0)	0.91	111.4	25.5
CS(2 $\rightarrow$ 1)	0.32	108.9	19.0
	0.24	104.2	1.4
CS(3 $\rightarrow$ 2)	0.37	108.9	20.0
CS(5 $\rightarrow$ 4)	0.35	108.5	15.6
CO(2 $\rightarrow$ 1)	17.6	111.1	22.5
	15.1	104.2	2.6
narrow-line position in shocked clump ( $-10''$ , $-85''$ ) <sup>b</sup>			
HCO <sup>+</sup> (1 $\rightarrow$ 0)	1.0	105.3	1.7
	0.38	102.6	14.4
CS(2 $\rightarrow$ 1)	0.90	105.5	1.0
	0.23:	103.7	6.0
CS(3 $\rightarrow$ 2)	0.55	105.4	1.2
	0.23	103.7	6.0
CS(5 $\rightarrow$ 4)	< 0.13		
CO(2 $\rightarrow$ 1)	11.6	105.5	1.2
	9.7	104.8	3.7
radio ridge ( $-130''$ , $+90''$ ) <sup>c</sup>			
HCO <sup>+</sup> (1 $\rightarrow$ 0)	0.22:	96.4	2.4
CS(2 $\rightarrow$ 1)	< 0.03		
CS(3 $\rightarrow$ 2)	< 0.04		
CS(5 $\rightarrow$ 4)	< 0.13		
CO(2 $\rightarrow$ 1)	8.9	96.5	4.0
	3.3	102.0	2.1
	3.6	107.0	3.8
clump in parent cloud ( $-130''$ , $+240''$ ) <sup>c</sup>			
HCO <sup>+</sup> (1 $\rightarrow$ 0)	0.32	96.1	7.3:
CS(2 $\rightarrow$ 1)	0.55	96.7	3.8
CS(3 $\rightarrow$ 2)	0.27	96.5	3.6
CS(5 $\rightarrow$ 4)	< 0.13		
CO(2 $\rightarrow$ 1)	12.0	96.0	5.4
	8.4	107.9	4.0

<sup>a</sup>only components between 90 and 140 km s<sup>-1</sup> are listed

<sup>b</sup>spectra averaged within 11'' radius

<sup>c</sup>spectra averaged within 21'' radius

## REFERENCES

Benson, P. J., Myers, P. C. 1989, ApJS, 71, 89

Borkowski, K. J., Blondin, J., Sarazin, C. L. 1992, ApJ, 4000, 222

Chevalier, R. A. 1977, ApJ, 213, 52

Clemens, D. P., Sanders, D. B., Scoville, N. Z., Solomon, P. M. 1986, ApJS, 60, 297

DeNoyer, L. K. 1983, ApJ, 264, 141

Downes, D., Wilson, T. L., Bieging, J., & Wink, J. 1980, A& AS, 40, 379

Draine, B. T., Roberge, W. G. 1984, ApJ, 282, 491

Elmegreen, B. G., Lada, C. J. 1977, ApJ, 214, 725

Esposito, J. A., Hunter, S. D., Kanbach, G., Sreekumar, P. 1996, ApJ, 461, 820

Falgarone, E., Panis, J.-F., Heithausen, A., Pérault, M., Stutzki, J., Puget, J.-L., & Bensch, F. 1998, A&A, 331, 669

Frail, D. A., Goss, W. M., Slysh, V. I. 1994, ApJ, 424, L111

Frail, D. A., Goss, W. M., Reynoso, E. M., Giacani, E. B., Green, A. J. 1996, AJ, 111, 1651

Green, D. A., Dewdney, P. E. 1992, MNRAS, 254, 686

Hester, J. J., Raymond, J. C., Blair, W. P. 1994, ApJ, 420, 721

Hollenbach, D., McKee, C. F. 1989, ApJ, 342, 306

Irvine, W. M., Goldsmith, P. F., & Hjalmarson, Å 1987, in *Interstellar Processes*, eds. D. J. Hollenbach & H. A. Thronson, Jr. (Kluwer: Dordrecht), p. 561

Koo, B.-C., Moon, D.-S. 1997a, ApJ, 475, 194

Koo, B.-C., Moon, D.-S. 1997b, ApJ, 485, 263

Mangum, J. G., Wootten, A. 1997, ApJS, 89, 123

Moorhouse, A., Brand, P. W. J. L., Geballe, T. R., Burton, M. G. 1991, MNRAS, 253, 662

Radakrishnan, V., Goss, W. M., Murray, J. D., & Brooks, J. W. 1972, ApJS, 24, 49

Reach, W. T., Pound, M. W., Wilner, D. J., & Lee, Y. 1995, ApJ, 441, 244

Reach, W. T., Rho, J. 1996, A&A, 315, L277

Reynolds, S. P., Moffett, D. A. 1993, AJ, 105, 2226

Rho, J., Petre, R. 1996, ApJ, 467, 698

Rho, J., Petre, R. 1998, ApJ, submitted

Seta, M. 1996, Ph. D. Thesis, University of Tokyo

Snell, R. L., Langer, W. D., Frerking, M. A. 1982, ApJ, 255, 149

Solomon, P. M., Rivolo, A. R., Barrett, J., Yahil, A. 1987, ApJ, 319, 730

Tatematsu, K., Fukui, Y., Iwata, T., Seward, F. D., Nakano, M. 1990, ApJ, 351, 157

van Dishoeck, E. F., Jansen, D. J., Phillips, T. G. 1993, A&A, 279, 541

Wang, Z., Scoville, N. Z. 1992, ApJ, 386, 158

White, G. J., Rainey, R., Hayashi, S. S., Kaifu, N. 1987, A&A, 173, 337

Wild, W. 1995, *The 30m Manual: A Handbook for the IRAM 30m Telescope, Pico Veleta, Spain*

Wilner, D. J., Reynolds, S. P., Moffett, D. A. 1998, AJ, 115, 247

Wootten, A. 1977, ApJ, 216, 440

Wootten, A. 1981, ApJ, 245, 105

Ziurys, L. M., Snell, R. L., & Dickman, R. L. 1989, ApJ, 341, 857